# Rechargeable nickel–iron batteries for large-scale energy storage

Abdallah H. Abdalla[1], Charles I. Oseghale[1], Jorge O. Gil Posada[1], Peter J. Hall[1] ✉

[1]Department of Chemical and Biological Engineering, Faculty of Engineering, University of Sheffield, Mappin Street, Sheffield S1 3JD, UK
✉ E-mail: peter.hall@sheffield.ac.uk

**Abstract:** This study reports the effect of iron sulphide and copper composites on the electrochemical performance of nickel–iron batteries. Nickel stripes were coated with an iron-rich electroactive paste and were cycled against commercial nickel electrodes. The electrodes electrochemical and physical characterisation were carried out by using galvanostatic charge/discharge, cyclic voltammetry, X-ray diffraction, and atomic force microscopy techniques. The authors' experimental results would indicate that the addition of iron sulphide and copper (II) sulphate significantly enhances the performance of the battery. Their in-house made iron-based electrodes exhibit good performance, with great potential for grid energy storage applications.

## 1 Introduction

The increasing demand for energy, depletion of supply of fossil fuels, and rising concerns over environmental pollution have encouraged the development and use of alternative, sustainable, and renewable energy resources [1–3]. Due to its natural environmental friendliness, abundance, renewable sources have the potential to reduce greenhouse gas emissions while offering a practical way of reducing our dependence on fossil fuels, it not surprising that most countries are taking serious steps to implement effective policies that will accelerate our use of such technologies [4, 5]. Moreover, it has been reported that the use of renewable energy continues to grow as global energy consumption increases. A staggering 19.1% of the global energy consumption during 2011–2012 was met by using renewable sources [6].

In recent years, renewable energy sources, such as the wind and solar power have emerged as a suitable solution to increase energy security, the supply of electricity, and mitigating environmental issues. Wind is a clean and non-polluting renewable source of energy that has received much attention for its potential to convert wind energy into more useful forms of energy such as electricity. Moreover, among all of the types of power production, renewable energy is considered as one of the fastest growing resources [6]. It is not surprising that in 2014, global wind energy production reached 370 GW, corresponding to an increase of almost 30% compared with the previous decade [6]. However, energy generation from renewable sources is not always possible when most needed (temporary wind profiles, seasonal availability of resources such as water, sunlight, etc.). Storing the energy during low load demand and then releasing it during the peak demand can overcome these problems. Combining renewable energy with energy storage, therefore, provides the natural solution to the asynchronous problem between energy generation from



**Fig. 1** *Schematic diagram of the battery-based interactive wind/solar power system*

intermittent power sources and demand [5]. Fig. 1 illustrates how energy storage could be used to help balance the electric grid.

Among various energy storage technologies, electrochemical energy storage has been identified as a practical solution that would help balance the electric grid by mitigating the asynchronous problem between energy generation and demand [5]. Moreover, electrochemical energy storage has been widely accepted as one of the most promising alternatives to store energy from intermittent power sources such as wind and solar for its high round-trip efficiency [5, 7, 8], long cycle life, low cost, high efficiency, and scalability [9, 10]. In the last century, several battery systems have been developed, but only a few have been demonstrated in large-scale applications. Among them, aqueous batteries have the potential to help balance the future electric grid at a lower cost than any of their non-aqueous counterparts (such as Li-ion, Na-ion, etc.) owing to its abundant raw materials and low-cost electrolyte (water based). Finally, non-aqueous batteries require costly safety systems to reduce the risk of arson; such expensive systems are not required with aqueous batteries [11–14].

Lead acid batteries are the earliest and well recognised as the leading technology for renewable applications, hence, their low energy density (about 30 Wh/kg), the toxicity of raw materials, and low cycle life [15, 16]. In contrast, invented and commercialised in the early 20th century, nickel–iron (NiFe) cells could provide 1.5–2 times the specific energy of lead/acid batteries, with their increased ruggedness and longer cycle life at deep discharge state (2000 cycles at 80% Depth of Discharge) [8, 11, 13, 16, 17]. In addition, NiFe batteries are well known for their long cycle life, typically exceeding 2000 cycles of charge and discharge [11, 18], vastly exceeding most of their competing technologies, this is lead/acid (300 cycles), nickel/cadmium (1500 cycles), and nickel metal hydride (500–800) [18].

Renewed interest in the iron-based batteries (such as NiFe) has been driven by the incentive to develop cost-effective, highly efficient energy storage technologies. NiFe cells are secondary batteries that are well known for robustness, non-toxicity, and eco-friendliness [19–22]. Besides, the relative abundance of chemicals and raw materials required to build these cells indicate that this technology could provide a cost-effective solution to store energy for grid system applications. However, the commercial deployment of these batteries has been limited by their poor charging efficiency (50–60%) and low discharge capability. These two problems are a direct consequence of the parasitic evolution of hydrogen that takes place during the charging of the battery. Considerable efforts have been devoted to overcoming the issues mentioned above.

In this regard, different effective approaches have been taken to counteract these issues, including using anode additives [23–27],
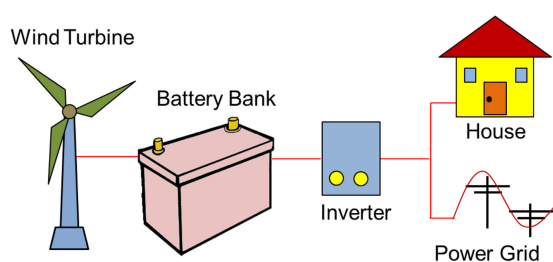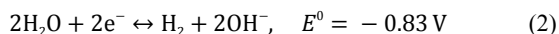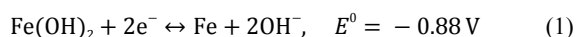
electrolyte additives [28–31], and nanosized Fe-based materials [8, 32–36]. Generally, all of them rely on either modifying the electrode formulation and/or tailoring the electrolyte [14, 24, 28, 31, 37, 38]. Under strong alkaline conditions, during the charging of an iron electrode, water is decomposed on its surface thus rendering hydrogen and hydroxyl groups, as shown in (2) [24, 38–42]

$$Fe(OH)_2 + 2e^- \leftrightarrow Fe + 2OH^-, \quad E^0 = -0.88\,V \quad (1)$$

$$2H_2O + 2e^- \leftrightarrow H_2 + 2OH^-, \quad E^0 = -0.83\,V \quad (2)$$

Due to electrolyte decomposition, part of the energy that was originally intended to be stored in the battery ended up wasted in decomposing the electrolyte. Mitigation or even prevention of hydrogen evolution is therefore crucial in achieving large-scale commercial implementation of these cells [14, 16, 31, 37]. Considering that many electrode additives such as bismuth, bismuth sulphide, cobalt, copper, and carbon-based materials have been tested, the addition of additives such as Na$_2$S, Li-ions to the electrolyte solution has also been reported as effective not only in controlling the reduction of Fe (III) to Fe(II) but also in increasing the capacity of the iron electrode as well [28, 43]. Table 1 reports figures of merit for selected anode systems for NiFe cells.
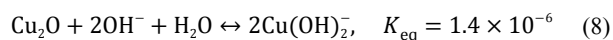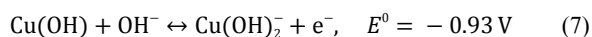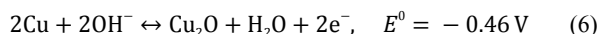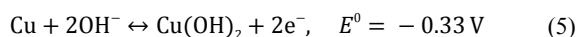
Recent studies have shown that selected electrode additives, such as bismuth and sulphur-containing species (including iron sulphide and bismuth sulphide), increase the activation barrier for water decomposition thus rendering a staggering tenfold reduction in the overall hydrogen evolution rate [8, 24, 44]. Besides, bismuth sulphide is electrically conducting and insoluble in aqueous solutions of potassium hydroxide. During the charging process of the cell, bismuth sulphide is reduced into elemental bismuth as represented by

$$Bi_2S_3 + 6e^- \leftrightarrow 2Bi + 3S^{2-}, \quad E^0 = -0.82\,V \quad (3)$$
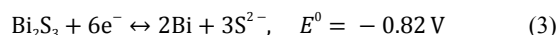
As per our knowledge, one of the less studied electrode additives with the potential to reduce the activation energy barrier for water decomposition on the surface of the iron electrode is copper. Moreover, copper is also well known for its high electrical conductivity, chemical activity, and reasonable price [45–50]. It has been observed that when placing together elemental iron in a solution of copper sulphate, a single replacement reaction as indicated by (4) would occur

$$Fe + CuSO_4 \leftrightarrow FeSO_4 + Cu \quad (4)$$
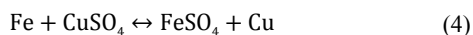
The formation of a protective layer of copper would act in a similar manner than the layer of elemental bismuth that was formed by (3). Moreover, the electrochemical behaviour of the Cu(II)/Cu(I) pair is reported to be similar to the Fe(III)/Fe(II) pair, as illustrated in (5)–(7) [46, 49, 51]

$$Cu + 2OH^- \leftrightarrow Cu(OH)_2 + 2e^-, \quad E^0 = -0.33\,V \quad (5)$$

$$2Cu + 2OH^- \leftrightarrow Cu_2O + H_2O + 2e^-, \quad E^0 = -0.46\,V \quad (6)$$

$$Cu(OH) + OH^- \leftrightarrow Cu(OH)_2^- + e^-, \quad E^0 = -0.93\,V \quad (7)$$

$$Cu_2O + 2OH^- + H_2O \leftrightarrow 2Cu(OH)_2^-, \quad K_{eq} = 1.4 \times 10^{-6} \quad (8)$$

It has been proposed that as the potential is increased beyond −0.4 V, the formation of Cu$_2$O (6) dominates over its dissolution (8) [51].

Electrolyte additives have also been used to enhance the performance of the battery. It has been reported that electrolyte systems based on Na$_2$S and LiOH would significantly improve the capacity of the iron electrode. It has been recently demonstrated that sulphide ions can suppress the electrolyte decomposition [28, 52, 53].

Nano-structuring the electrodes is another approach that has rendered high-performance batteries; this approach has been successfully implemented not only in the area of Li-ion batteries but also in producing aqueous batteries [35]. With all of this in mind, we aim to explore the use of different forms of copper (metallic and copper sulphate) and iron sulphide as electrode additives for suppressing the evolution of hydrogen; likewise, we shall also use potassium sulphide as an electrolyte additive to further improve our in-house made NiFe cells.

This manuscript aims to clarify the effect of iron sulphide and copper composites in suppressing the evolution of hydrogen in the electrolyte, thus improving the overall performance of the NiFe cells.

## 2 Experimental

Strips of nickel foam (4 cm × 1 cm) were coated with differing amounts of electrode materials. An electroactive paste consisting of iron powder (Fe, 99% ≤ 10 μm, Sigma-Aldrich), mixed with differing amounts of iron sulphide (FeS, 99.5% ≤ 10 μm, Sigma-Aldrich), copper sulphate (CuSO$_4$ 5H$_2$O, 98% ≤ 10 μm, Alfa Aesar), and polytetrafluroethylene (PTFE) (Teflon 30-N, 59.95% solids, Alfa Aesar) were used. The mixture was then homogenised for 10 min on an ultrasonic bath, applied to the nickel foam (Ni, purity 99.0%, density 350 g/m$^2$, Sigma-Aldrich), and vacuum dried for 5 h at 100°C. The coating process was repeated until a constant amount of iron was reached (about 300 mg/cm$^2$). The electrodes were vacuum dried overnight to ensure consistency. A brief description of electrode preparation procedures and testing was described by Yang *et al.* [54].

To efficiently investigate the effect of different concentration of sulphur-containing additives while keeping a reasonable number of experiments, a full factorial design was used and in order to ensure consistency, three replicates per formulation were used. Table 2 shows the experimental factors and level used during the experiment.

By considering the mixing rules in a four-dimensional (4D) composition space and based on the constancy of PTFE, a 2$^2$ full factorial design with four replicates per formulation for a total of 16 runs were used.

Data extraction was automated by using an in-house developed C/C++ program that interrogates all files produced by the battery cycles, the data thus obtained was analysed by utilising Python and the r statistical software. More experimental design details can be found here [42].

Cells were assembled into a three-electrode cell configuration, where a commercial nickel electrode was used as a counter electrodes (CE), our in-house made pasted electrodes were used as the working electrode, and a mercury/mercury oxide (MMO) was

**Table 1** Selected anode systems for NiFe cells[a]

| Materials | Particle size, μm | Support materials | Additives | Design | Capacity, Ah/g | Charging efficiency | Ref. |
|---|---|---|---|---|---|---|---|
| Fe | 1–3 | none | none | pressed pocket-plate | 0.12 (C/5) | 70 (C/20) | [44] |
| Fe | 1–3 | none | 4.5% Bi$_2$S$_3$ | powder spread + PTFE | 0.33 (C/5) | 33 (C/5) | [42] |
| Fe + Fe$_3$O$_4$ | 5–10 | PVA + CC | 1.0% Bi$_2$S$_3$ | powder spread + PTFE | 0.4 (C/5) | 80 (C/5) | [12] |
| carbonyl Fe | 0.5–3 | none | 10% Bi$_2$O$_3$+FeS | pressed powder + PP | 0.22 (C/5) | 93 (C/20) | [25] |
| carbonyl Fe | 0.5–3 | none | 5.0% Bi$_2$S$_3$ | pressed powder +PP | 0.24 (C/5) | 30 (C/5) | [24, 39] |

CC, carbon black; PP, polyethylene powder; PTFE, polytetrafluroethylene; PVA, polyvinyl alcohol.
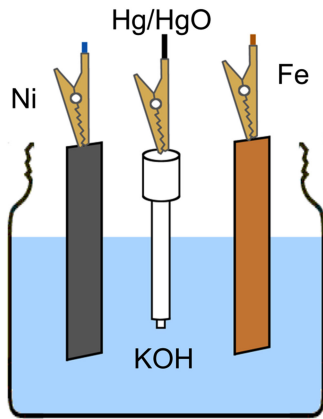
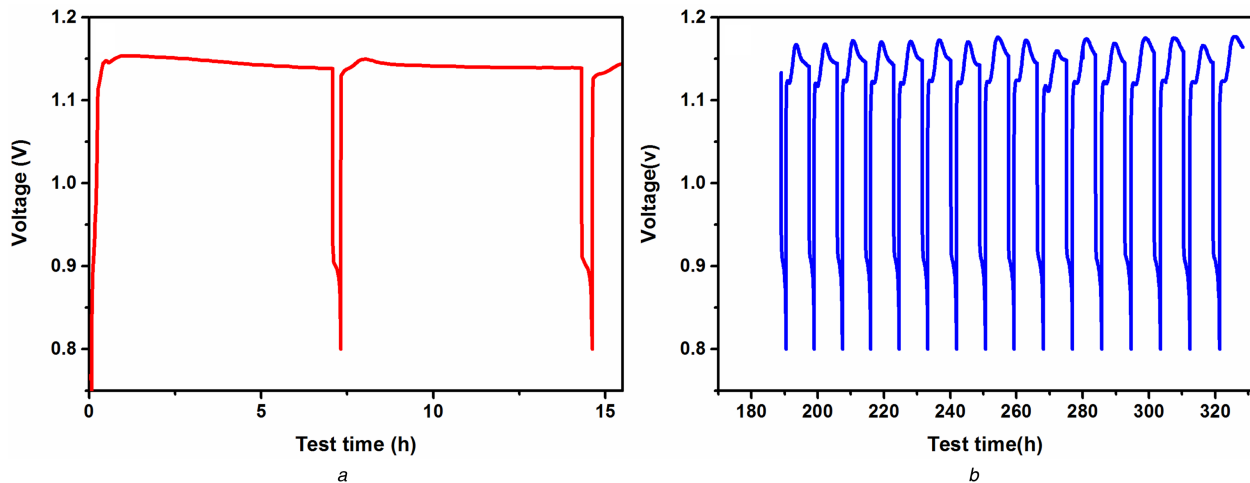**Fig. 2** *Schematic diagram of the cell configuration*



**Fig. 3** *Typical charge and discharge voltage profiles of a NiFe cell*
*(a)* Galvanostatic charge–discharge curves of the first and second cycles of an iron electrode versus Hg/HgO RE at C/5 rate, *(b)* Charge–discharge curves of the cycles from 17th–35th among 60 cycles

charge used for hydrogen evolution was calculated with the current of hydrogen evolution, which in turn was calculated by using the Tafel relationship [55].

Cyclic voltammetry (CV) was conducted under potentiostatic control using an eight-channel Solartron 1470E/1455A potentiostat/galvanostat. The electrochemical measurements were made using a conventional three-electrode glass cell. The RE was Hg/HgO ($E_{Hg/HgO}$ = +0.098 V versus the standard hydrogen electrode) and the CE was a platinum wire. CV experiments of the Fe–Cu rich paste were conducted at room temperature on aqueous solutions of KOH.

X-ray diffraction (XRD) was used to characterise the electrode and determine the crystal phase of the materials. X-ray data were obtained on a Bruker D2 Phaser system with Cu-Kα, $\lambda$ = 1.5406 nm radiation, and step time of 0.1 s in a $2\theta$ at the range between 0 and 85°($2\theta$); detector set to 0.27 V of the lower detection limit. The XRD data analysis was performed by the International Centre for Diffraction Data (ICDD) PDF-4+ and Sieve+ software.

used as reference electrode (RE) ($E_{Hg/HgO}$ = +0.098 V versus normal hydrogen electrode). The electrolyte was an aqueous solution of 28.5 w/v% KOH (purity ≥ 85.0%, pellets, Sigma-Aldrich). In-house deionised water was produced by using an Elix 10-Milli-Q Plus water purification system (Millipore, Eschborn, Germany). Iron electrodes were cycled under galvanostatic conditions for 60 cycles to their rated capacity (0.35 Ah/g) at C/5 rate from −0.8 to −1.4 V versus MMO RE at laboratory temperature. The electrochemical tests were carried out using a 64-Channel Arbin SCTS battery cycler operating under galvanostatic conditions. A sketch of the cell test configuration can be found in Fig. 2.

The efficiency of the battery was calculated by using the following expression:

$$\eta_Q = \frac{Q_{ch} - Q_H}{Q_{ch}} \times 100 \qquad (9)$$

where $\eta_Q$ is the coulombic efficiency, $Q_{ch}$ is the total charge, and $Q_H$ is the charge wasted in electrolyte decomposition [8]. The

**Table 2** Main factors and levels used in experiment (electrode material compositions in weight per cent)

| Factors | Level, %$_w$ | |
| --- | --- | --- |
| | Low | High |
| Fe | 82 | 89 |
| FeS | 0 | 5 |
| CuSO$_4$ | 3 | 5 |
| PTFE | 8 | 8 |

Atomic force microscopy (AFM) was used to investigate the surface morphology at the iron electrodes before and after cycling. After cycled, electrodes were immediately rinsed with deionised water, followed by drying under stream nitrogen. AFM imaging was performed on Bruker Dimension Icon, operating with the ScanAsyst system in soft tapping mode in air, and the height of images was attained by using a silicon cantilever, with the nominal force constant of 40 N/m, and resonant frequency of 300 kHz.

## 3 Result and discussion

### 3.1 Galvanostatic cycling

As was explained, batteries were cycled at room temperature until they reached the steady state (usually 25–30 cycles) [14], so meaningful comparisons could be drawn. Typical charge and discharge voltage profiles of a NiFe cell can be found in Fig. 3a. It has been reported that NiFe cells require a conditioning period before they reached their full potential [14, 24, 37, 38, 42]; so it makes sense to expect a similar behaviour for iron electrode formulations utilising copper. Fig. 3b confirms this hypothesis as it clearly indicates that cell performance increases with the cycle number.

The practical implications of Fig. 3 are tremendous as it confirms the use of copper sulphate in the electrode increases the overall performance of the NiFe cell. Formulations lacking copper tend to exhibit extremely low coulombic efficiencies (1–5%, results not shown). However, in the presence of copper sulphate, coulombic efficiencies increase up to eight times.

Our experimental results demonstrate the usefulness of copper sulphate as an electrode additive for improving the performance of iron electrodes. Fig. 4 clearly indicates that the use of copper sulphate has a positive effect on increasing both the coulombic
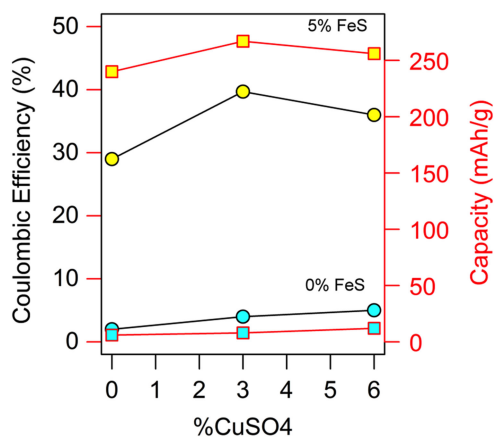
**Fig. 4** *Battery performance as a function of composition. Squares and circles denote capacity and coulombic efficiency, respectively. Likewise, cyan and yellow colours indicate compositions of 0% (curves on a lower part of the diagram) and 5% (curves on an upper part of the diagram), respectively, of FeS*
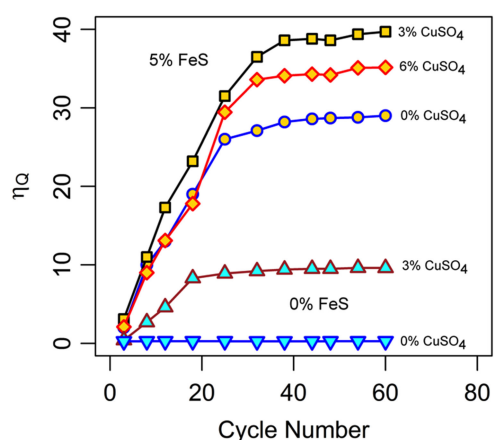


**Fig. 5** *Coulombic efficiency versus cycle number for selected electrode formulations. The lower curves on the diagram (cyan colour) correspond to 0% FeS; likewise, the upper curves (gold) correspond to 5% FeS*
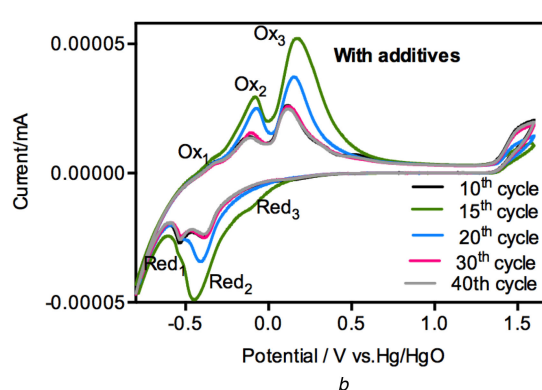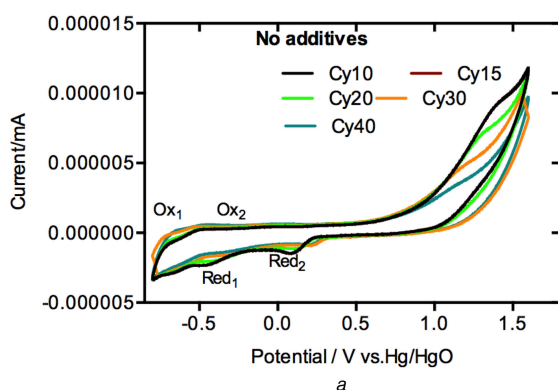


**Fig. 6** *CV for the paste-type iron electrode*
*(a)* Without additives, *(b)* With additives

exhibits a relatively low coulombic efficiency of about 30%. However, the addition of copper sulphate to the same formulation renders nearly 10% increases in battery performance ($\eta_Q \simeq 40\%$) (Fig. 5).

From our experimental results, it follows that the addition of copper sulphate increases the performance of the battery, by preventing electrolyte decomposition. This observation holds in the concentration range from between 0 and 6% of $CuSO_4$. The authors believe that this might be due to the formation of a copper layer on different sectors of the iron electrode, this iron copper would increase the activation barrier for electrolyte decomposition, thus increasing the overall performance of the iron electrode.

Broadly speaking, electrode formulations based on $CuSO_4$ outperformed their plain iron-based counterparts. However, at the confidence level $\alpha = 0.05$, we have found no meaningful formulations based on 3 and 6% of $CuSO_4$. This would indicate that more research is still needed to determine the concentration space where cell performance is being maximised.

Although we have developed formulations that decrease the evolution of hydrogen, our formulations exhibit a decrease in capacity after the 15th cycle, so we also propose to investigate the use of additives like bismuth sulphide, which increases the performance and stability of NiFe cells. It has been proposed, however, that the reduction of electrode capacity can be counteracted by the addition of sodium sulphide to the electrolyte [28], so it is worth exploring the incidence of this compound as a means to increase cell performance. Finally, our experimental observations confirm that iron electrodes tend to fall apart with the cycle number; this observation has been reported many times before [24, 28, 42]. The authors believe the manufacturing process can still further be refined or even replaced by using different binders or manufacturing approaches.

### 3.2 Cyclic voltammetry

The CV experiments of the iron electrode with and without copper additives are shown in Fig. 6. In Fig. 6*a*, the forward scan (oxidation curve) for electrodes without additives reveals two oxidative peaks at −0.92 V $Fe/Fe(OH)_2$ and −0.78 V for $Fe(OH)_2/Fe(III)$, respectively [34, 49, 56]. As confirmed in Fig. 6*b*, there are three oxidation/reduction peaks, peak 1 (Ox1) at −0.38 V which is associated with the oxidation of $Cu/Cu_2O$, peak 2 (Ox2) with

efficiency and the capacity of the iron electrode. In fact, under the experimental conditions explored here, it seems like there is an optimal composition for copper sulphate in the nearness of $3\%_w$ $CuSO_4$, but more investigation is still required to optimise the formulation. It is also apparent that the presence of iron sulphide tends to increase the performance of the battery to a larger extent than copper sulphate. In fact, very high-performance FeS-based batteries have already been reported [37].

The specific discharge capacities for our iron electrodes with and without additive as a function of the cycle number are shown in Fig. 4. Also, as can be seen, the formulation based on FeS

$Cu_2O/CuO$ at potential of −0.12 V, and the third anodic peak with $CuO/Cu(OH)_2$ at 0.6 V. These strong oxidation peaks implies their high reversibility at a high current density. Finally, the strong oxidative peak at −0.78 V implies the oxidation of $Fe(OH)_2$ to $Fe_3O_4$, this final observation was confirmed by the XRD analysis.

### 3.3 Characterisation of the electrodes

The XRD pattern reveals strong signals indicating well-crystallised peaks at $2\theta$ values corresponding to the main phases of Fe matched with the standard ICDD card no: 006-0696, FeS ICDD card no:
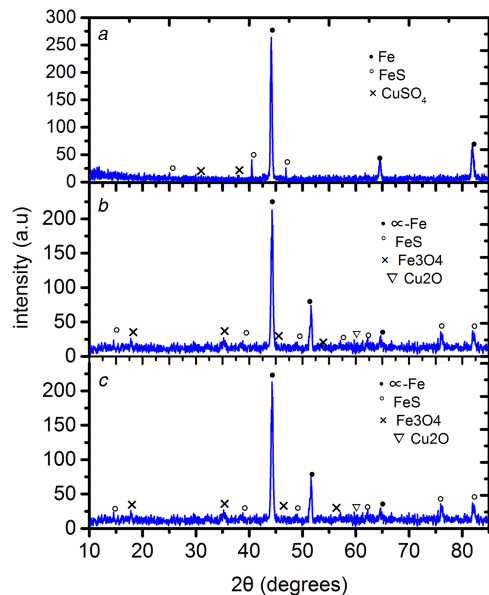
**Fig. 7** *X-ray powder diffraction pattern for the iron electrode*
*(a)* Before charging, *(b, c)* After charging
Powder diffraction cards: Fe (00-006-0696), $Fe_3O_4$ (00-065-0731), FeS (04-003-01443), $CuSO_4$ (01-077-1900), $Cu_2O$ (01-078-2076)

copper centres on the surface of the electrolyte (as suggested by (4)); note that electrolyte decomposition of water is not favoured on copper as is of iron, so the overall performance of the battery is increased. The XRD analysis of our samples confirms the formation of $Fe_3O_4$ during the discharge reaction.

To investigate the surface morphology of the electrodes, AFM was used to study the structure of our samples. Fig. 8 shows AFM 3D images of iron electrodes before and after cycling. The average surface roughness evaluated over the 3D surface before and after 60 cycles of charge and discharge was 2.69 and 21.0 nm, respectively. Finally, the AFM analysis would also suggest that the surface of the electrode deteriorates with the cycle number; this observation is in line with the fact that electrodes tend to fall apart (to some extent) when cycled.

## 4 Conclusion

Aiming to develop highly efficient NiFe cells for offshore wind applications, iron electrodes based on Fe/FeS/$CuSO_4$ were investigated. Our experimental results indicate that copper sulphate increases the performance of iron-based electrodes in the range between 0 and 6%. Likewise, we could confirm that the presence of iron sulphide in the electrode has a real incidence on its performance; basically, the addition of iron sulphide has a much greater influence than using copper alone. AFM and visual inspection have confirmed that the cycling of electrodes under strong alkaline conditions would most certainly compromise the structural integrity of the cells. Coulombic efficiencies in the order
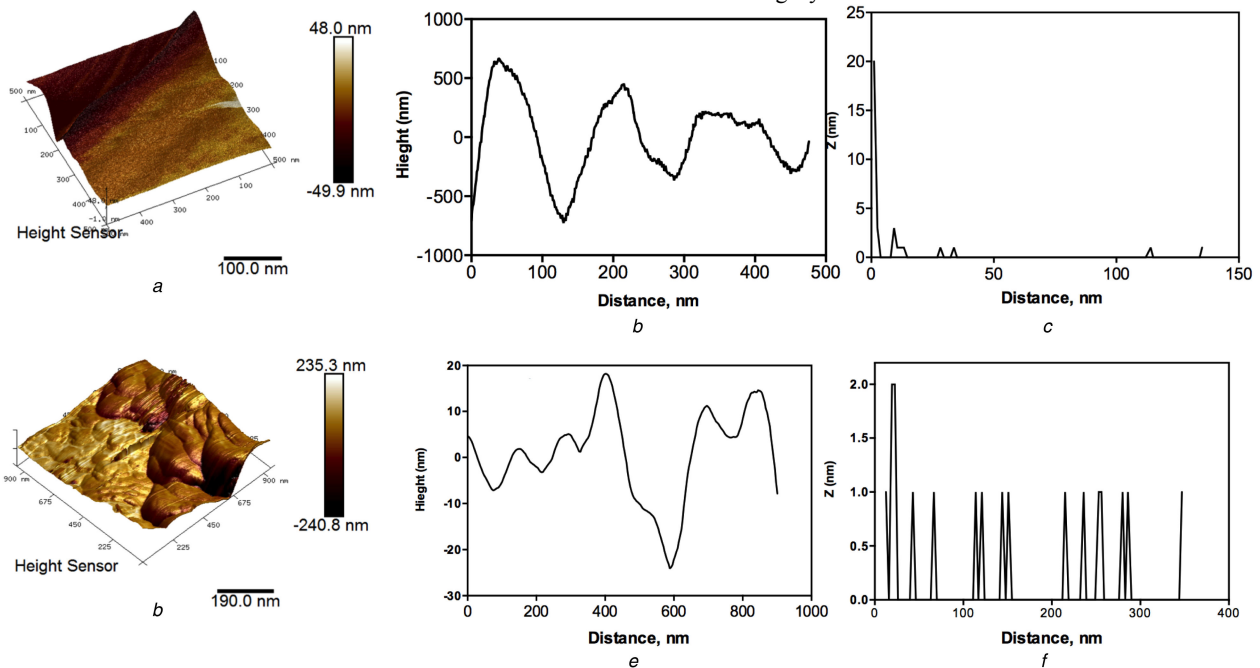


**Fig. 8** *Soft tapping-mode AFM images*
*(a)* Height sensor image of the iron powder electrode with additive before discharge/charge cycling, *(b–e)* Cross-section along the line in phase image, *(c–f)* Corresponding phase image, *z*-range, *(d)* Height sensor of the image iron powder electrode with additives after 60 cycles of charge and discharge

04-003-1443, $Cu_2O$ ICDD card no: 01-078-2076, $Fe_3O_4$ ICDD card no: 00-065-0731, and $CuSO_4$ ICDD card no: 01-077-1900, respectively. It is worth nothing that after cycling, electrodes exhibited strong iron signals of higher intensity than their non-cycled counterparts.

As can be shown from Figs. 7*b* and *c*, the formation of $Fe_3O_4$ is much stronger after the deep cycling. It is also worth noting that $Fe_3O_4$ was produced during the discharge reaction, as confirmed by the AFM image morphology (see Fig. 8). The $Cu_2O$ observed peaks are indicative that the copper was oxidised (as shown by (6)) at the deep discharge state [34].

It is important to understand that, broadly speaking, our evidence is in line with our initial claim that copper (in the form of copper sulphate) would modify in some way the activation energy for electrolyte decomposition, probably by rendering metallic

of 40% and enormous capacities exceeding 300 mA/g were found. It is important to mention that we have used commercial grade reactants and materials only, so this technology has the potential to be a cost-effective energy storage solution for large-scale applications.

## 5 Acknowledgments

# 6 References

[1] Sarrias-Mena, R., Fernández-Ramírez, L.M., García-Vázquez, C.A., *et al.*: 'Improving grid integration of wind turbines by using secondary batteries', *Renew. Sustain. Energy Rev.*, 2014, **34**, pp. 194–207

[2] Warren, P.: 'A review of demand-side management policy in the UK', *Renew. Sustain. Energy Rev.*, 2014, **29**, (0), pp. 941–951

[3] Oseghale, C.I., Abdalla, A.H., Posada, J.O.G., *et al.*: 'A new synthesis route for sustainable gold copper utilization in direct formic acid fuel cells', *Int. J. Hydrog. Energy*, 2016, **41**, pp. 16394–16401

[4] Hollister-Short, G.: '*History of technology*' (Bloomsbury Publishing, 2016)

[5] Zhao, H., Wu, Q., Hu, S., *et al.*: 'Review of energy storage system for wind power integration support', *Appl. Energy*, 2015, **137**, pp. 545–553

[6] network, T.g.r.e.p.: 'Renewables 2015 Global Status Report', 2015

[7] Narayanan, S.R., Prakash, G.K.S., Manohar, A., *et al.*: 'Materials challenges and technical approaches for realizing inexpensive and robust iron–air batteries for large-scale energy storage', *Solid State Ion.*, 2012, **216**, pp. 105–109

[8] Manohar, A.K., Malkhandi, S., Yang, B., *et al.*: 'A high-performance rechargeable iron electrode for large-scale battery-based energy storage', *J. Electrochem. Soc.*, 2012, **159**, (8), pp. A1209–A1214

[9] Alotto, P., Guarnieri, M., Moro, F.: 'Redox flow batteries for the storage of renewable energy: a review', *Renew. Sustain. Energy Rev.*, 2014, **29**, pp. 325–335

[10] Chen, H., Cong, T.N., Yang, W., *et al.*: 'Progress in electrical energy storage system: a critical review', *Prog. Nat. Sci.*, 2009, **19**, (3), pp. 291–312

[11] Poullikkas, A.: 'A comparative overview of large-scale battery systems for electricity storage', *Renew. Sustain. Energy Rev.*, 2013, **27**, pp. 778–788

[12] Rajan, A.S., Sampath, S., Shukla, A.K.: 'An in situ carbon-grafted alkaline iron electrode for iron-based accumulators', *Energy Environ. Sci.*, 2014, **7**, (3), pp. 1110–1116

[13] Liu, J., Zhang, J.-G., Yang, Z., *et al.*: 'Materials science and materials chemistry for large scale electrochemical energy storage: from transportation to electrical grid', *Adv. Funct. Mater.*, 2013, **23**, (8), pp. 929–946

[14] Gil Posada, J.O., Abdalla, A.H., Oseghale, C.I., *et al.*: 'Multiple regression analysis in the development of NiFe cells as energy storage solutions for intermittent power sources such as wind or solar', *Int. J. Hydrog. Energy*, 2016, **41**, pp. 16330–16337

[15] Vela, N., Aguilera, J.: 'Characterisation of charge voltage of lead-acid batteries: application to the charge control strategy in photovoltaic systems', *Prog. Photovolt., Res. Appl.*, 2006, **14**, (8), pp. 721–732

[16] Gil Posada, J.O., Rennie, A.J.R., Villar, S.P., *et al.*: 'Aqueous batteries as grid scale energy storage solutions', *Renew. Sustain. Energy Rev.*, 2016, in press, corrected proof

[17] Wilson, I.A.G., McGregor, P.G., Hall, P.J.: 'Energy storage in the UK electrical network: estimation of the scale and review of technology options', *Energy Policy*, 2010, **38**, (8), pp. 4099–4106

[18] Vijayamohanan, K., Balasubramanian, T.S., Shukla, A.K.: 'Rechargeable alkaline iron electrodes', *J. Power Sources*, 1991, **34**, (3), pp. 269–285

[19] Wang, H., Liang, Y., Gong, M., *et al.*: 'An ultrafast nickel–iron battery from strongly coupled inorganic nanoparticle/nanocarbon hybrid materials', *Nat. Commun.*, 2012, **3**, p. 917

[20] Shukla, A.K., Venugopalan, S., Hariprakash, B.: 'Nickel-based rechargeable batteries', *J. Power Sources*, 2001, **100**, (1–2), pp. 125–148

[21] Öjefors, L.: 'Self-discharge of the alkaline iron electrode', *Electrochim. Acta*, 1976, **21**, (4), pp. 263–266

[22] Öjefors, L., Carlsson, L.: 'An iron–air vehicle battery', *J. Power Sources*, 1978, **2**, (3), pp. 287–296

[23] Manohar, A.K., Yang, C., Narayanan, S.R.: 'Effect of sulfide additives on the discharge characteristics of iron electrodes in alkaline batteries', *Meet. Abs.*, 2016, **MA2016-01**, (3), p. 390

[24] Gil Posada, J.O., Hall, P.J.: 'Post-hoc comparisons among iron electrode formulations based on bismuth, bismuth sulphide, iron sulphide, and potassium sulphide under strong alkaline conditions', *J. Power Sources*, 2014, **268**, (0), pp. 810–815

[25] Manohar, A.K., Yang, C., Malkhandi, S., *et al.*: 'Enhancing the performance of the rechargeable iron electrode in alkaline batteries with bismuth oxide and iron sulfide additives', *J. Electrochem. Soc.*, 2013, **160**, (11), pp. A2078–A2084

[26] Egashira, M., Kushizaki, J.-Y., Yoshimoto, N., *et al.*: 'The effect of dispersion of nano-carbon on electrochemical behavior of Fe/nano-carbon composite electrode', *J. Power Sources*, 2008, **183**, (1), pp. 399–402

[27] Hang, B.T., Yoon, S.-H., Okada, S., *et al.*: 'Effect of metal-sulfide additives on electrochemical properties of nano-sized $Fe_2O_3$-loaded carbon for Fe/air battery anodes', *J. Power Sources*, 2007, **168**, (2), pp. 522–532

[28] Posada, J.O.G., Hall, P.J.: 'The effect of electrolyte additives on the performance of iron based anodes for NiFe cells', *J. Electrochem. Soc.*, 2015, **162**, (10), pp. A2036–A2043

[29] Yang, B., Malkhandi, S., Manohar, A.K., *et al.*: 'Organo-sulfur molecules enable iron-based battery electrodes to meet the challenges of large-scale electrical energy storage', *Energy Environ. Sci.*, 2014, **7**, (8), pp. 2753–2763

[30] Hang, B.T., Watanabe, T., Egashira, M., *et al.*: 'The effect of additives on the electrochemical properties of Fe/C composite for Fe/air battery anode', *J. Power Sources*, 2006, **155**, (2), pp. 461–469

[31] Posada, J.O.G., Hall, P.J.: 'Controlling hydrogen evolution on iron electrodes', *Int. J. Hydrog. Energy*, 2016, in press, corrected proof

[32] Shangguan, E., Li, F., Li, J., *et al.*: 'FeS/C composite as high-performance anode material for alkaline nickel–iron rechargeable batteries', *J. Power Sources*, 2015, **291**, pp. 29–39

[33] Huo, G., Lu, X., Huang, Y., *et al.*: 'Electrochemical performance of A-$Fe_2O_3$ particles as anode material for aqueous rechargeable batteries', *J. Electrochem. Soc.*, 2014, **161**, (6), pp. A1144–A1148

[34] Kao, C.-Y., Tsai, Y.-R., Chou, K.-S.: 'Synthesis and characterization of the iron/copper composite as an electrode material for the rechargeable alkaline battery', *J. Power Sources*, 2011, **196**, (13), pp. 5746–5750

[35] Kao, C.-Y., Chou, K.-S.: 'Iron/carbon-black composite nanoparticles as an iron electrode material in a paste type rechargeable alkaline battery', *J. Power Sources*, 2010, **195**, (8), pp. 2399–2404

[36] Hang, B.T., Watanabe, T., Eashira, M., *et al.*: 'The electrochemical properties of $Fe_2O_3$-loaded carbon electrodes for iron–air battery anodes', *J. Power Sources*, 2005, **150**, pp. 261–271

[37] Posada, J.O.G., Hall, P.J.: 'Towards the development of safe and commercially viable nickel–iron batteries: improvements to coulombic efficiency at high iron sulphide electrode formulations', *J. Appl. Electrochem.*, 2016, **46**, (4), pp. 451–458

[38] Posada, J.O.G., Hall, P.J.: 'Surface response investigation of parameters in the development of FeS based iron electrodes', *Sustain. Energy Technol. Assess.*, 2015, **11**, (0), pp. 194–197

[39] Haddad, F., Eddine Amara, S., Kesri, R.: 'Liquidus surface projection of the Fe–Co–C ternary system in the iron-rich corner', *Int. J. Mater. Res.*, 2008, **99**, (9), pp. 942–946

[40] Benhalla-Haddad, F., Amara, S.E., Benchettara, A., *et al.*: 'Contribution to the study of the relation between microstructure and electrochemical behavior of iron-based FeCoC ternary alloys', *J. Anal. Methods Chem.*, 2012, **2012**, pp. 798043–798046

[41] Hall, D.S., Lockwood, D.J., Bock, C., *et al.*: 'Nickel hydroxides and related materials: a review of their structures, synthesis and properties', *Proc. R. Soc. London A, Math. Phys. Eng. Sci.*, 2015, **471**, (2174), 1364–1429

[42] Gil Posada, J.O., Hall, P.J.: 'Multivariate investigation of parameters in the development and improvement of NiFe cells', *J. Power Sources*, 2014, **262**, (0), pp. 263–269

[43] Ujimine, K., Tsutsumi, A.: 'Electrochemical characteristics of iron carbide as an active material in alkaline batteries', *J. Power Sources*, 2006, **160**, (2), pp. 1431–1435

[44] Manohar, A.K., Yang, C.G., Malkhandi, S., *et al.*: 'Understanding the factors affecting the formation of carbonyl iron electrodes in rechargeable alkaline iron batteries', *J. Electrochem. Soc.*, 2012, **159**, (12), pp. A2148–A2155

[45] Kim, J.-K., Nishikata, A., Tsuru, T.: 'Influence of copper on iron corrosion in weakly alkaline environment containing chloride ions', *Mater. Trans.*, 2003, **44**, (3), pp. 396–400

[46] Paixão, T.R.L.C., Ponzio, E.A., Torresi, R.M., *et al.*: 'EQCM behavior of copper anodes in alkaline medium and characterization of the electrocatalysis of ethanol oxidation by Cu(III)', *J. Braz. Chem. Soc.*, 2006, **17**, pp. 374–381

[47] Shan, J., Pulkkinen, P., Vainio, U., *et al.*: 'Synthesis and characterization of copper sulfide nanocrystallites with low sintering temperatures', *J. Mater. Chem.*, 2008, **18**, (27), pp. 3200–3208

[48] Chou, K.-S., Kao, C.-Y.: 'Iron/copper composite nanoparticles as iron electrode material in rechargeable alkaline battery', *Meet. Abs.*, 2009, **MA2009-02**, (5), p. 269

[49] Jayalakshmi, M., Balasubramanian, K.: 'Cyclic voltammetric behavior of copper powder immobilized on paraffin impregnated graphite electrode in dilute alkali solution', *Int. J. Electrochem. Sci.*, 2008, **3**, (11), pp. 1277–1287

[50] Lv, P., Wang, Z.-M., Peng, Y., *et al.*: 'Effect of Cu content on structure, hydrogen storage properties and electrode performance of Lani4.1-X Co0.6mn0.3cu X alloys', *J. Solid State Electrochem.*, 2014, **18**, (9), pp. 2563–2572

[51] Giri, S.D., Sarkar, A.: 'Electrochemical study of bulk and monolayer copper in alkaline solution', *J. Electrochem. Soc.*, 2016, **163**, (3), pp. H252–H259

[52] Burke, L.D., Nugent, P.F.: 'The electrochemistry of gold: II the electrocatalytic behaviour of the metal in aqueous media', *Gold Bull.*, 1998, **31**, (2), pp. 39–50

[53] Burke, L.D., Nugent, P.F.: 'The electrochemistry of gold: I the redox behaviour of the metal in aqueous media', *Gold Bull.*, 1997, **30**, (2), pp. 43–53

[54] Yang, Q.M., Ettel, V.A., Babjak, J., *et al.*: 'Pasted Ni (Oh) 2 electrodes using Ni powders for high-drain-rate, Ni-based batteries', *J. Electrochem. Soc.*, 2003, **150**, (4), pp. A543–A550

[55] Balasubramanian, T.S., Shukla, A.K.: 'Effect of metal-sulfide additives on charge/discharge reactions of the alkaline iron electrode', *J. Power Sources*, 1993, **41**, (1–2), pp. 99–105

[56] Černý, J., Micka, K.: 'Voltammetric study of an iron electrode in alkaline electrolytes', *J. Power Sources*, 1989, **25**, (2), pp. 111–122